


Cite this: *RSC Adv.*, 2022, 12, 72

Effect of calcination temperature and Ti substitution on optical properties of $(\text{Fe,Cr})_2\text{O}_3$ cool black pigment prepared by spray pyrolysis

Jin Soo Hwang and Kyeong Youl Jung *

Near-infrared (NIR) reflective $\text{Fe}_{1.5}\text{Cr}_{0.5}\text{O}_3$ black pigments were synthesized by spray pyrolysis, and the effect of calcination temperature and Ti substitution on the optical properties were investigated. As the calcination temperature increased from 500 °C to 800 °C, the prepared $\text{Fe}_{1.5}\text{Cr}_{0.5}\text{O}_3$ powder had $\alpha\text{-Fe}_2\text{O}_3$ phase without any impurities and the NIR reflectance steadily increased. On the otherhand, the smallest chroma value was observed at 700 °C. Therefore, in terms of achieving high NIR reflectance with keeping good blackness, the optimal calcination temperature was determined to be 700 °C. Substitution of Ti corresponding to 5–15% of the total metal ions in $\text{Fe}_{1.5}\text{Cr}_{0.5}\text{O}_3$ largely affected the NIR reflectance and chroma value, but there was no significant change in the optical band gap. Ti substitution of 5 mol% could further improve the NIR reflectance of the $\text{Fe}_{1.5}\text{Cr}_{0.5}$ black pigment without significant loss of blackness, but above 10% or higher the NIR reflectance largely decreased due to the loss of crystallinity. Resultantly, $\text{Fe}_{1.4}\text{Cr}_{0.5}\text{Ti}_{0.1}\text{O}_{3+\delta}$ (5% Ti substituted black pigment) was confirmed to have improved heat-shielding performance compared to $\text{Fe}_{1.5}\text{Cr}_{0.5}\text{O}_3$ in a temperature rise test under near-infrared illumination.

Received 12th November 2021
Accepted 14th December 2021

DOI: 10.1039/d1ra08300g

rsc.li/rsc-advances

Introduction

Cool pigments, which effectively reflect near-infrared (NIR) rays from sunlight, are attracting great attention because they can effectively prevent indoor temperature rise in summer and reduce the effect of urban heat islands.^{1,2} Heat accumulation is mainly caused by dark pigments, especially black pigments painted on the roof or the roadway surface. The natural sunlight is known to consist of 5% ultraviolet (UV), 43% visible light and 52% near-infrared (NIR).³ The NIR absorption of dark pigments mainly causes the indoor temperature rise. One of the most effective ways to control the heat from sunlight is to paint cool pigments with high NIR reflectance on the exterior walls of residential or office buildings. Therefore, designing new achromatic inorganic pigments with high NIR reflection is necessary and important to reduce heat build-up in buildings.

TiO_2 , ZnO , Fe_2O_3 and Cr_2O_3 are representative NIR-reflective inorganic pigments.^{4–6} TiO_2 is white and has excellent reflectivity for both visible and NIR light. However, when only TiO_2 pigment is used, it is too bright and has strong glare, which is unpleasant to human eyes. Fe_2O_3 and Cr_2O_3 are red and green pigments with high NIR reflection, respectively. Therefore, both have been used as key components of various colored inorganic pigments with high NIR reflection. In special, Cr-doped iron

oxide ($\text{Fe}_{2-x}\text{Cr}_x\text{O}_3$) is a potential inorganic black pigment and has good NIR reflection properties.^{7,8}

Mixing TiO_2 with other colored organic pigments is a simple way to enhance the NIR reflectivity. However, although the physical mixing of TiO_2 can improve the NIR reflectance, it is impossible to maintain the original color of the inorganic pigments. Recently, Sadeghi-Niaraki *et al.* synthesized Fe/Cr/Ti-based cool pigments with different hues and good NIR reflectance.⁹ They reported that the $(\text{Fe,Cr})_2\text{O}_3@ \text{TiO}_2$ core-shell shows higher NIR reflectance than physically mixed $\text{Fe}_2\text{O}_3\text{-Cr}_2\text{O}_3$ or $\text{Fe}_2\text{O}_3\text{-Cr}_2\text{O}_3\text{-TiO}_2$ pigments. However, CIE $L^*a^*b^*$ colorimetric parameters of $(\text{Fe,Cr})_2\text{O}_3@ \text{TiO}_2$ core-shell are largely different with that of $(\text{Fe,Cr})_2\text{O}_3$ black. Thus, a new approach is needed to prepare Fe–Cr–Ti–O black pigments having improved NIR reflectivity while maintaining blackness. Despite many efforts, to our best knowledge, there is no report of improving the NIR reflectivity of $(\text{Fe,Cr})_2\text{O}_3$ black pigments without significant color change.

In multi-component pigments, the distribution of each component, powder crystallinity and phase purity are crucial factors influencing the optical properties. Such factors strongly depend on the synthesis method of pigments. Until now, $(\text{Fe,Cr})_2\text{O}_3$ has been synthesized by a conventional solid-state reaction or a liquid-phase precipitation.^{4,10} Spray pyrolysis, one of the gas phase synthesis techniques, has been used to make a variety of functional materials.^{11–16} In spray pyrolysis, one particle is produced from one droplet containing all precursors. As a result, all ingredients can be mixed at the

Department of Chemical Engineering, Kongju National University, 1224-24 Cheonan-Daero, Seobuk-gu, Cheonan, Chungnam 31080, Republic of Korea. E-mail: kjjung@kongju.ac.kr



nanoscale. Nevertheless, to the best of our knowledge, there are no reports of investigation of the synthesis and optical properties of $(\text{Fe,Cr})_2\text{O}_3$ pigments using spray pyrolysis. In this work, spray pyrolysis was applied to the preparation of $(\text{Fe,Cr})_2\text{O}_3$ and Ti-substituted $(\text{Fe,Cr})_2\text{O}_3$ pigments applicable as a cool pigment. The effects of post-heat treatment on crystal structure, color coordinates and NIR reflectance were investigated, and the performance of the prepared pigments as cool pigments was evaluated by temperature rise test under NIR illumination. The goal of this study is to find the optimal synthetic conditions of $(\text{Fe,Cr})_2\text{O}_3$ black pigment and to investigate whether the NIR reflectance of $(\text{Fe,Cr})_2\text{O}_3$ can be improved by Ti substitution while maintaining blackness.

Experimental

$\text{Fe}_{1.5}\text{Cr}_{0.5}\text{O}_3$ and $\text{Fe}_{1.5-x}\text{Cr}_{0.5}\text{Ti}_x\text{O}_{3+\delta}$ black pigments were synthesized by spray pyrolysis. $\text{Fe}(\text{NO}_3)_3 \cdot 9\text{H}_2\text{O}$, $\text{Cr}(\text{NO}_3)_3 \cdot 9\text{H}_2\text{O}$ and $\text{Ti}[\text{OCH}(\text{CH}_3)_2]_4$ (titanium(IV) isopropoxide, TTIP) were used as precursors for pigment synthesis. The precursor solution was prepared by dissolving each precursor in purified water. When preparing a precursor solution of $\text{Fe}_{1.5-x}\text{Cr}_{0.5}\text{Ti}_x\text{O}_{3+\delta}$, TTIP was first slowly added to purified water (250 ml) with nitric acid (15 ml) and vigorously mixed with a magnetic stirrer until the solution became transparent. Then, Fe and Cr precursors were added to the TTIP dissolved solution, and purified water was added to adjust the total solution volume to 500 ml. The molar concentration of the precursor solution was fixed to 0.3 M, and the Ti content (x) in $\text{Fe}_{1.5-x}\text{Cr}_{0.5}\text{Ti}_x\text{O}_{3+\delta}$ was changed from 0.1 to 0.3. The prepared precursor aqueous solution was converted into droplets using an ultrasonic nebulizer consisting of six vibrators of 1.7 MHz, and the resulting droplets were injected into a quartz reactor (ID = 55 mm, L = 1200 mm) of 900 °C using air (30 liter min^{-1}) as a carrier gas. The precursor powder produced through a drying and pyrolysis process of droplets was collected using a Teflon bag filter connected to the end of the quartz reactor and calcined while flowing air in a tube furnace at a different temperature of 500 to 800 °C.

X-ray diffraction (XRD) patterns were obtained using X-ray diffractometer (MiniFlex600, Rigaku) in order to identify the crystal structure of the calcined pigment powders. Scanning electron microscopy (SEM) (Hitachi S-4800), transmission electron microscopy (TEM) (JEM-2100F, JEOL) and elemental mapping analysis were performed to investigate the particle shape and microstructure, and the distribution of each component. A UV-Vis-NIR spectrophotometer (Cary 5000 UV-Vis-NIR, Agilent) was used to obtain the reflection spectra of each sample in visible and near-infrared region. From the measured reflectance and standard solar irradiation (ASTM G173-03), the total infrared reflectance (R_{NIR}) was calculated using the following equations.

$$R_{\text{NIR}} = \frac{\int_{700}^{2500} r(\lambda) i(\lambda) d\lambda}{\int_{700}^{2500} i(\lambda) d\lambda} \quad (1)$$

where $i(\lambda)$ is the standard solar irradiation (ASTM G173-03) and $r(\lambda)$ is the reflection value of each sample. The $L^*a^*b^*$ color

coordinates of the prepared pigments were measured using a spectrophotometer (YS3030), and the chroma (C^*) value was calculated using the formula $C^* = (a^{*2} + b^{*2})^{1/2}$. To evaluate the NIR performance, a temperature rise test was performed under irradiation with an infrared lamp (IR 250 RH IR2 230V 250W, PHILIPS) for the pigment film which was formed on an aluminium plate (10 cm × 10 cm) using a doctor blade method.

Results and discussion

Fig. 1 shows the XRD patterns of Fe_2O_3 and $\text{Fe}_{1.5}\text{Cr}_{0.5}\text{O}_3$ powder prepared by spray pyrolysis and calcined at different temperatures. The observed diffraction peaks are well matched to a standard pattern (JCPDS# 01-080-2377) of $\alpha\text{-Fe}_2\text{O}_3$ without any impurities regardless of the calcination temperature. This XRD result indicates that the Cr^{3+} ions do not form independent chromium oxide crystals in the $\alpha\text{-Fe}_2\text{O}_3$ matrix. As shown in Fig. 1(a) and (b), the diffraction peak observed for $\text{Fe}_{1.5}\text{Cr}_{0.5}\text{O}_3$ is the same as that of Fe_2O_3 . The diffraction peak position of $\text{Fe}_{1.5}\text{Cr}_{0.5}\text{O}_3$ is shifted to the right compared to Fe_2O_3 , indicating that Cr^{3+} ions are well substituted into the hematite unit cells. As increasing the temperature, the crystallinity increases, so the width of the peak narrows and the intensity increases. The contribution of crystallite size (D) and lattice strain to the broadening of diffraction peaks can be expressed by the following Williamson–Hall (W–H) equation.¹⁷

$$\beta_{hkl} \cos \theta = \frac{K\lambda}{D_{\text{W-H}}} + 4\epsilon \sin \theta \quad (2)$$

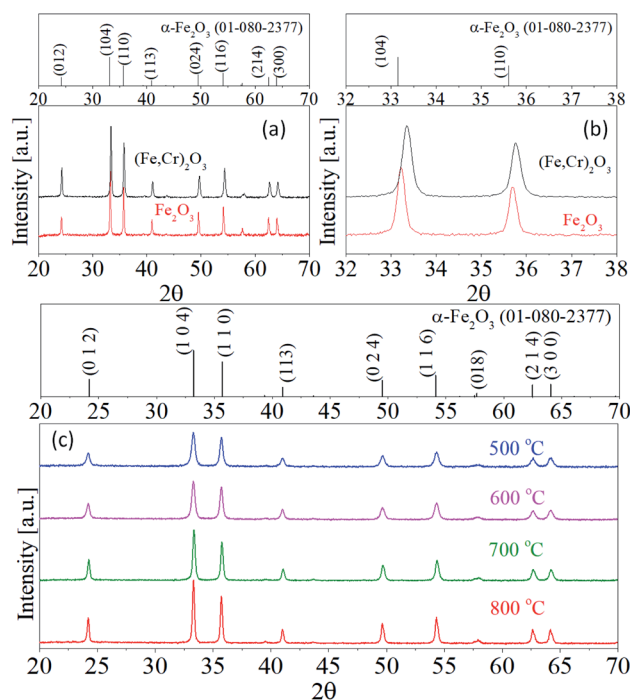


Fig. 1 (a) XRD patterns and (b) enlarge view of XRD pattern of (104) and (110) plane for Fe_2O_3 and $\text{Fe}_{1.5}\text{Cr}_{0.5}\text{O}_3$. (c) XRD patterns of $\text{Fe}_{1.5}\text{Cr}_{0.5}\text{O}_3$ calcined at different temperatures.

where ε is the microstrain, β_{hkl} corresponds to the full width at half maximum (FWHM) of the diffraction peak for the (hkl) plane, K is the shape factor ($K = 0.9$), λ is the Cu K α radiation wavelength (0.1549 nm) and D_{W-H} is crystallite size. The crystallite size and the microstrain can be obtained from the intercept ($K\lambda/D_{W-H}$) and the slope (4ε) in the W-H plot of $\beta_{hkl} \cos \theta$ versus $\sin \theta$, respectively. W-H plots were performed using XRD peaks for the lattice planes of (012), (104), (110), (113), (024), (116), 214 and (300), and the results are shown in Fig. 2(a). The resulting crystallite size and microstrain are summarized in Table 1. Both crystallite size (D_{W-H}) and microstrain increase with increasing calcination temperature up to 700 °C. At 800 °C, the microstrain decreases without significant change in crystallite size. The increase of the lattice strain is due to the substitution of Cr ions into the Fe sites of Fe_2O_3 crystal lattice. One notable thing is that the lattice strain increases significantly at 700 °C, which indicates that Cr^{3+} was well substituted into the Fe^{3+} sites. At 800 °C, however, the macro-strain is smaller than at 700 °C. The lattice constant and unit cell volume of hematite Fe_2O_3 were calculated from the XRD patterns. Fig. 2(b) and (c) show the dependence of the unit cell volume and the lattice constants on the calcination temperature. The unit cell volume slightly decreases as the calcination temperature increases up to 700 °C. At 800 °C, however, the unit cell volume increases again. The same temperature dependence is observed in the lattice constant a and c values as shown in Fig. 2(c). The unit cell contraction is due to the substitution of Fe^{3+} (ionic radius = 0.069 Å) by Cr^{3+} (ionic radius = 0.0615 nm). At 800 °C, the increase of the unit cell volume indicates that some Cr^{3+} ions escape from the hematite unit cell.

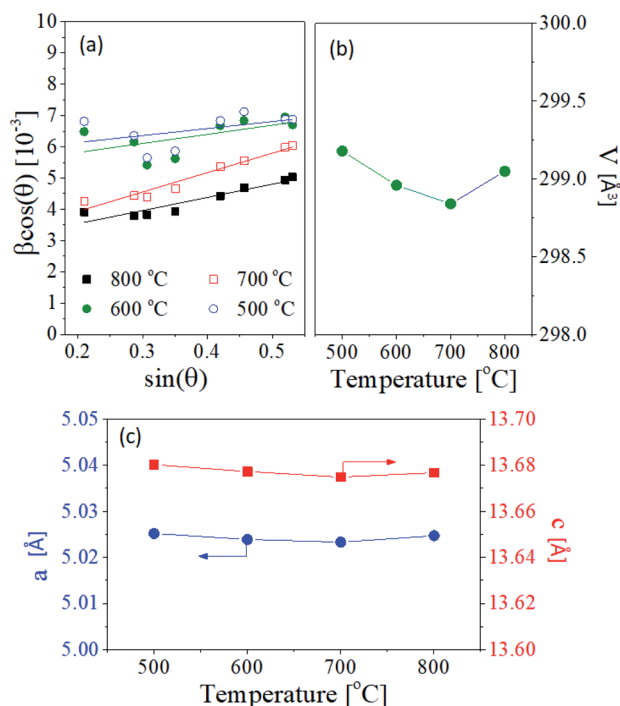


Fig. 2 (a) W-H plot, (b) unit cell volume and (c) lattice constant of $\text{Fe}_{1.5}\text{Cr}_{0.5}\text{O}_3$ pigments calcined at different temperatures.

The $L^*a^*b^*$ color coordinates of $\text{Fe}_{1.5}\text{Cr}_{0.5}\text{O}_3$ pigments are summarized in Table 1, and Fig. 3 shows the photographs of the $\text{Fe}_{1.5}\text{Cr}_{0.5}\text{O}_3$ pigments calcined at the temperature from 500 °C to 800 °C. The color of the as-prepared sample is close to brown and turns to black after calcining at 600 °C and 700 °C. When calcined at 800 °C, the $\text{Fe}_{1.5}\text{Cr}_{0.5}\text{O}_3$ pigment is a slightly reddish black. The a^* and b^* values of the $\text{Fe}_{1.5}\text{Cr}_{0.5}\text{O}_3$ pigment slightly decrease as the calcination temperature increases to 700 °C. Resultantly, the chroma (C^*) value decreases to 700 °C and slightly increases at 800 °C. In terms of preparing achromatic pigments, the lower the C^* value, the better. Thus, the calcination at 700 °C is required to obtain $\text{Fe}_{1.5}\text{Cr}_{0.5}\text{O}_3$ black pigment with good blackness *via* spray pyrolysis.

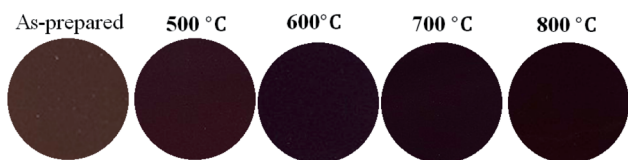
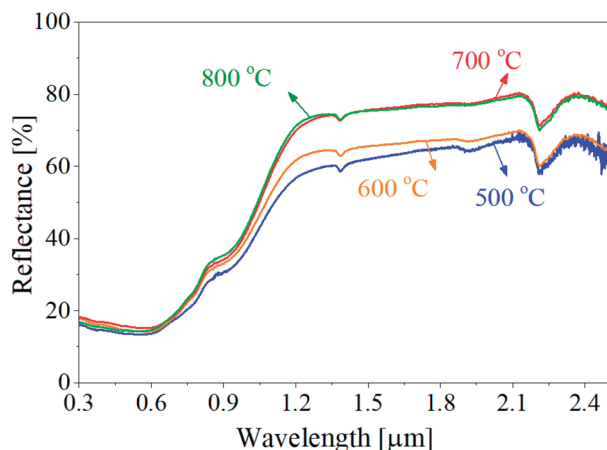
Fig. 4 shows the UV-Vis-NIR reflectance of $\text{Fe}_{1.5}\text{Cr}_{0.5}\text{O}_3$ black pigments calcined at different temperatures. In the UV-visible region, there is no significant change in the reflectance with varying the calcination. On the other hand, in the NIR region, the reflectance steadily increase up to 700 °C. The total NIR reflectance (R_{NIR}) of $\text{Fe}_{1.5}\text{Cr}_{0.5}\text{O}_3$ calcined at different temperatures was calculated by the eqn (1), and the resulting values were summarized in Table 1. The NIR reflectance increases from 41.1% to 49.1% as the calcination temperature increases from 500 °C to 800 °C. At 700 °C, the NIR reflectance is about 48.5%, which is 0.6% lower than at 800 °C. From the optical data for chroma value and NIR reflectance, the optimum calcination temperature was determined to be 700 °C, because it is more important to achieve improvement of NIR reflectance while minimizing the blackness loss.

To improve the NIR reflectance, Ti^{4+} atoms were introduced to the Fe^{3+} site of $\text{Fe}_{1.5}\text{Cr}_{0.5}\text{O}_3$ matrix. Fig. 5 shows the photographs of the resulting pigments prepared at different chemical composition of $(\text{Fe}_{1.5-x}\text{Cr}_{0.5}\text{Ti}_x\text{O}_{3+\delta})$. At $x = 0.1$, the pigment has no significant change in power color. However, at $x = 0.3$, the $(\text{Fe}_{1.2}\text{Cr}_{0.5}\text{Ti}_{0.3}\text{O}_{3+\delta})$ color changes to a reddish black. The $L^*a^*b^*$ color coordinates of $(\text{Fe}_{1.5-x}\text{Cr}_{0.5}\text{Ti}_x\text{O}_{3+\delta})$ pigments are measured and summarized in Table 2. Compared to $\text{Fe}_{1.5}\text{Cr}_{0.5}\text{O}_3$ ($x = 0.0$), the sample with $x = 0.1$ has slightly larger L^* value, while the a^* and b^* values are smaller. However, when the Ti content (x) is more than 0.2, the L^* value decreases and the a^* and b^* values increase again. Therefore, Ti substitution of less than 5% ($x = 0.1$) of the total amount of cationic metal does not cause a substantial change in powder color, and there is no problem in obtaining achromatic pigment.

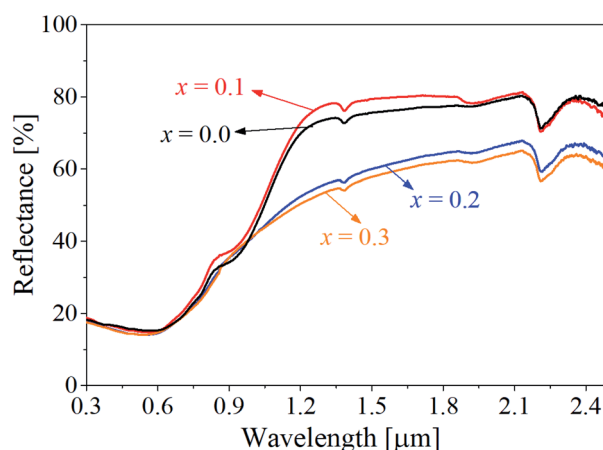
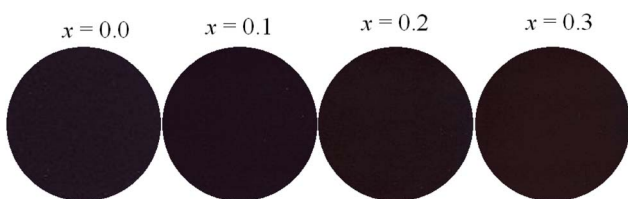
Fig. 6 is the UV-Vis-NIR diffuse reflectance of $\text{Fe}_{1.5-x}\text{Cr}_{0.5}\text{Ti}_x\text{O}_{3+\delta}$ pigment powder. There is no significant change in the reflectance at the UV and visible region. On the other hand, in the NUV region, the reflectance of $\text{Fe}_{1.5-x}\text{Cr}_{0.5}\text{Ti}_x\text{O}_{3+\delta}$ shows a big difference depending on the Ti content. The total NIR reflectance with varying the Ti content is summarized in Table 2. The $\text{Fe}_{1.5-x}\text{Cr}_{0.5}\text{Ti}_x\text{O}_{3+\delta}$ pigment having the Ti content of $x = 0.1$ has a higher NIR reflectance than $\text{Fe}_{1.5}\text{Cr}_{0.5}\text{O}_3$. For the pigments with the Ti content of $x = 0.2$ and 0.3, however, the NIR reflectance is largely reduced. The band gap (E_g) of $\text{Fe}_{1.5-x}\text{Cr}_{0.5}\text{Ti}_x\text{O}_{3+\delta}$ was estimated from the UV-Vis-NIR diffuse reflectance using the Kubelka-Munk equation and Tauc plot. Fig. 7 is the Tauc plot for each sample. The resulting band gap value is about 1.65 ± 0.02 eV. That is, there is no significant

Table 1 Crystallite size, lattice strain, color coordinates and total NIR reflectance (R_{NIR}) of $\text{Fe}_{1.5}\text{Cr}_{0.5}\text{O}_3$ pigments prepared by spray pyrolysis and calcined at different temperatures

Temp. [$^{\circ}\text{C}$]	Crystallite size [nm]	Microstrain, ε [10^{-4}]	Optical properties				
	$D_{\text{W-H}}$		L^*	a^*	b^*	C^*	R_{NIR} [%]
500	24.1	5.6	27.72	2.73	0.55	2.78	41.1
600	26.2	7.3	24.04	2.54	−0.18	2.55	44.0
700	51.0	15.6	23.77	2.23	−0.06	2.23	48.5
800	50.9	10.5	24.34	2.65	0.52	2.70	49.1

**Fig. 3** Photographs of $\text{Fe}_{1.5}\text{Cr}_{0.5}\text{O}_3$ powder prepared by spray pyrolysis and calcined at different temperature.**Fig. 4** UV-Visible-NIR diffuse reflectance of $\text{Fe}_{1.5}\text{Cr}_{0.5}\text{O}_3$ pigment powder prepared by spray pyrolysis and calcined at different temperatures.**Table 2** $L^*a^*b^*$ color coordinates of $\text{Fe}_{1.5-y}\text{Cr}_{0.5}\text{Ti}_y\text{O}_{3+\delta}$ pigment powders prepared spray pyrolysis at different Ti content

Ti content [x]	L^*	a^*	b^*	C^*	R_{NIR} [%]
0	24.04	2.54	−0.18	2.55	48.5
0.1	25.50	2.01	0.10	2.01	50.9
0.2	23.08	2.56	0.42	2.59	41.8
0.3	23.01	2.98	0.86	3.10	40.8

**Fig. 6** UV-Visible-NIR diffuse reflectance of $\text{Fe}_{1.5-x}\text{Cr}_{0.5}\text{Ti}_x\text{O}_{3+\delta}$ pigment powder prepared by spray pyrolysis and calcined at 700 $^{\circ}\text{C}$.**Fig. 5** Photographs of $\text{Fe}_{1.5-x}\text{Cr}_{0.5}\text{Ti}_x\text{O}_{3+\delta}$ particles prepared by spray pyrolysis and calcined at 700 $^{\circ}\text{C}$.

change in the band gap as the Ti content changes. This result indicates that the Ti introduction up to about 15% of the total amount of cationic metal does not significantly affect the optical band gap of $\text{Fe}_{1.5-x}\text{Cr}_{0.5}\text{Ti}_x\text{O}_{3+\delta}$. Therefore, in terms of maximizing the NIR reflectance of black pigments while

keeping the blackness, the optimal Ti content is 5.0 mol% ($x = 0.1$) of the total cationic elements in $\text{Fe}_{1.5-x}\text{Cr}_{0.5}\text{Ti}_x\text{O}_{3+\delta}$.

Fig. 8 shows the XRD pattern of $\text{Fe}_{1.5-x}\text{Cr}_{0.5}\text{Ti}_x\text{O}_{3+\delta}$ powder calcined at 700 $^{\circ}\text{C}$. The observed diffraction peaks are well matched with $\alpha\text{-Fe}_2\text{O}_3$ (JCPDS# 01-080-2377). As shown in Fig. 8(a), the diffraction peak intensity of $\alpha\text{-Fe}_2\text{O}_3$ decreases significantly with increasing Ti content. Regardless of the Ti content, no peaks for impurities are observed, indicating that the added Ti element does not participate in the crystal formation of TiO_2 or iron titanate compounds. Fig. 8(b) is the diffraction peak for the (110) crystal plane of Fe_2O_3 . The (104) peak slightly shifts to a larger diffraction angle, which is due to the substitution of Ti^{4+} (ionic radius = 0.061 nm) into the Fe^{3+} (ionic radius = 0.069 nm) site of $\alpha\text{-Fe}_2\text{O}_3$. From the XRD analysis, the Ti addition cause a reduction in the crystallinity of



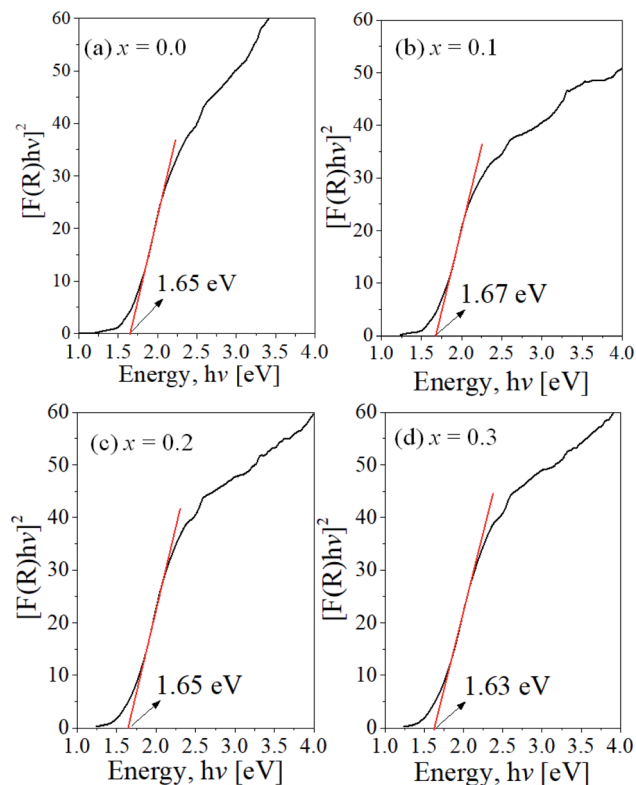


Fig. 7 Tauc plot for $(\text{Fe}_{1.5-x}\text{Cr}_{0.5}\text{Ti}_x\text{O}_{3+\delta})$ powder with different Ti content.

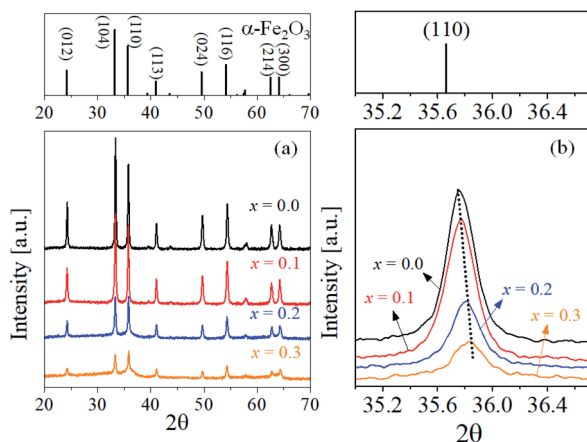


Fig. 8 XRD patterns of $(\text{Fe}_{1.5-x}\text{Cr}_{0.5}\text{Ti}_x\text{O}_{3+\delta})$ powder with different Ti content: (a) at wide diffraction angle and (b) for the (110) phase.

pigment powder. In special, when the Ti content (x value) is 2 or larger, a large reduction in crystallinity occurs. According to the results of XRD and NIR reflectance analysis for the $\text{Fe}_{1.5}\text{Cr}_{0.5}\text{O}_3$ powder calcined at different temperature, the higher in the crystallinity, the higher in the NIR reflectance. Thus, the large reduction in the NIR total reflectance when the Ti content is above 10.0% ($x = 2$) is due to the reduction of crystallinity.

To investigate the microstructure of the $\text{Fe}_{1.4}\text{Cr}_{0.5}\text{Ti}_{0.1}\text{O}_{3+\delta}$ sample, SEM and TEM analysis was performed, and the

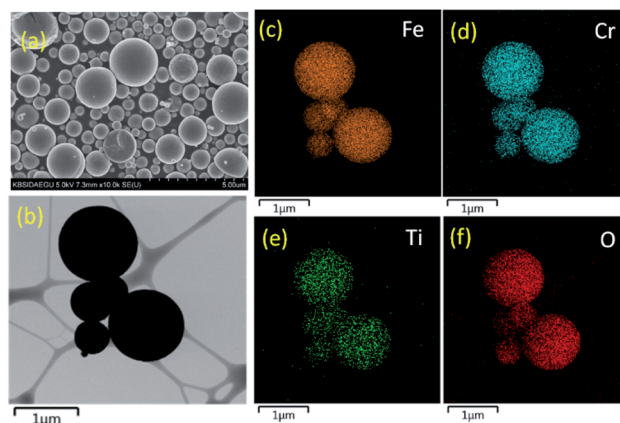


Fig. 9 SEM (a), TEM (b) and element mapping (c–f) of $\text{Fe}_{1.4}\text{Cr}_{0.5}\text{Ti}_{0.1}\text{O}_{3+\delta}$ pigment powder.

resulting photos are shown in Fig. 9. The prepared pigment powder has a spherical shape of fine size, typically observed in particles synthesized by a spray pyrolysis process. Furthermore, the particles show a dense structure, indicating that a volumetric precipitation of salts occurs during the droplet drying step. When spray pyrolysis is applied to synthesize multi-component ceramic powder, all components can be

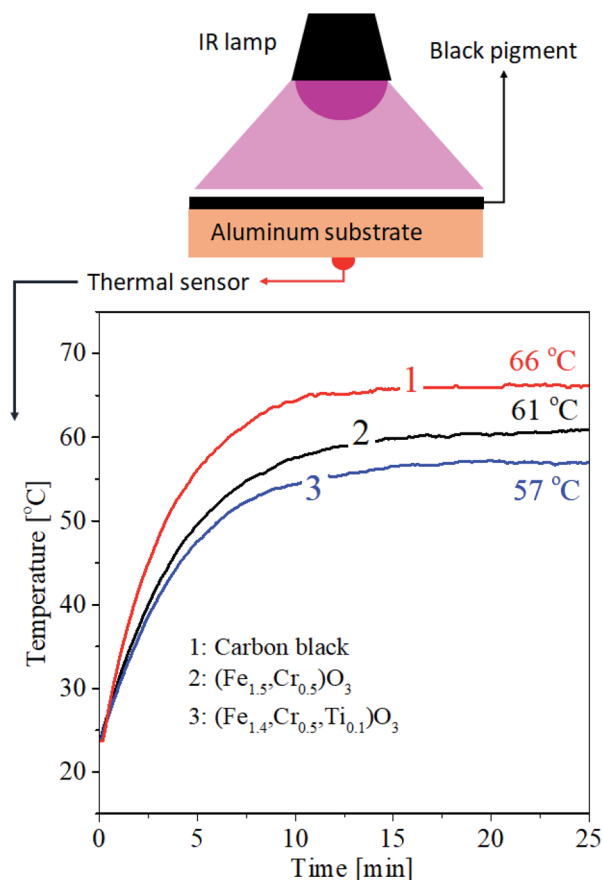


Fig. 10 Temperature change as a function of IR illumination time.



homogeneously mixed in the entire particle. Fig. 9(c)–(f) are the element mapping results, confirming that Cr and Ti elements are uniformly distributed throughout the particle.

$\text{Fe}_{1.5}\text{Cr}_{0.5}\text{O}_3$, $\text{Fe}_{1.4}\text{Cr}_{0.5}\text{Ti}_{0.1}\text{O}_{3+\delta}$ and commercially-available carbon black pigments were coated on an aluminium plate, and a temperature rise test was performed to see the effectiveness of the NIR reflectance improvement. Fig. 10 shows the temperature of the black pigment film as a function of the IR illumination time. The temperature of each pigment-coated plate rapidly increases and reaches an equilibrium. The commercial carbon black has the equilibrium temperature of about 66 °C. On the other hand, $\text{Fe}_{1.5}\text{Cr}_{0.5}\text{O}_3$ and $\text{Fe}_{1.4}\text{Cr}_{0.5}\text{Ti}_{0.1}\text{O}_{3+\delta}$ give equilibrium temperatures of 61 °C and 57 °C, respectively. That is, the prepared inorganic black pigment has better NIR reflectance than carbon black. In addition, the temperature rise of $\text{Fe}_{1.4}\text{Cr}_{0.5}\text{Ti}_{0.1}\text{O}_{3+\delta}$ is smaller than that of $\text{Fe}_{1.5}\text{Cr}_{0.5}\text{O}_3$, which well reflects the improvement of NIR reflection by the Ti substitution into the $\text{Fe}_{1.5}\text{Cr}_{0.5}\text{O}_3$ matrix.

Conclusions

The effect of calcination temperature or Ti substitution on the optical properties of $\text{Fe}_{1.5}\text{Cr}_{0.5}\text{O}_3$ cool black pigment was investigated. The prepared $\text{Fe}_{1.5}\text{Cr}_{0.5}\text{O}_3$ particles had a crystal-line phase of $\alpha\text{-Fe}_2\text{O}_3$ without any impurities regardless of the change in the calcination temperature of 500 to 800 °C. As the calcination temperature increased up to 700 °C, the L^* and chroma (C^*) values of $\text{Fe}_{1.5}\text{Cr}_{0.5}\text{O}_3$ decreased because of improved substitution of Cr ions into $\alpha\text{-Fe}_2\text{O}_3$ unit cells. When preparing $\text{Fe}_{1.5}\text{Cr}_{0.5}\text{O}_3$ black pigment with good blackness and high NIR reflectance through spray pyrolysis, the optimum calcination temperature was determined to be 700 °C. Ti substitution (5–15%) at the Fe site of $\text{Fe}_{1.5}\text{Cr}_{0.5}\text{O}_3$ induced large change in chroma values and NIR reflectance, although there was no significant change in the optical band gap of the resulting pigment. It was found that Ti substitution of 5 mol% ($x = 0.1$) in the $\text{Fe}_{1.5}\text{Cr}_{0.5}\text{O}_3$ matrix could further improve the NIR reflectance while minimizing blackness loss. As a result, in the temperature rise test under near-infrared illumination, the Ti-substituted pigment ($\text{Fe}_{1.4}\text{Cr}_{0.5}\text{Ti}_{0.1}\text{O}_{3+\delta}$) had improved heat-shielding performance compared to $\text{Fe}_{1.5}\text{Cr}_{0.5}\text{O}_3$.

Conflicts of interest

There are no conflicts to declare.

Acknowledgements

This research was supported by the Industrial Technology Innovation Program (Grant no. 20004663) funded by the Ministry of Trade, Industry & Energy (MI, Korea) and partially supported by Basic Science Research Program through the National Research Foundation of Korea (NRF) funded by the Ministry of Education (Grant no. 2021R1F1A1062022).

References

- 1 A. Rosati, M. Fedel and S. Rossi, *J. Cleaner Prod.*, 2021, **313**, 127826.
- 2 M. Santamouris, *Renewable Sustainable Energy Rev.*, 2013, **26**, 224–240.
- 3 R. Oka, S. Iwasaki and T. Masui, *RSC Adv.*, 2019, **9**, 38822–38827.
- 4 S. Sadeghi-Niaraki, B. Ghasemi, A. Habibolahzadeh, E. Ghasemi and M. Ghahari, *Mater. Chem. Phys.*, 2019, **235**, 121769.
- 5 D. Lu, Q. Gao, X. Wu and Y. Fan, *Ceram. Int.*, 2017, **43**, 9164–9170.
- 6 D. N. Hebbar, K. S. Choudhari, S. A. Shivashankar, C. Santhosh and S. D. Kulkarni, *J. Alloys Compd.*, 2019, **785**, 747–753.
- 7 R. Levinson, P. Berdahl and H. Akbari, *Sol. Energy Mater. Sol. Cells*, 2005, **89**, 351–389.
- 8 Á. G. De la Torre and M. A. G. Aranda, *Int. J. Appl. Ceram. Technol.*, 2011, **8**, 905–910.
- 9 S. Sadeghi-Niaraki, B. Ghasemi, A. Habibolahzadeh, E. Ghasemi and M. Ghahari, *J. Alloys Compd.*, 2019, **779**, 367–379.
- 10 A. Escardino, S. Mestre, A. Barba, V. Beltrán and A. Blasco, *J. Am. Ceram. Soc.*, 2000, **83**, 29–32.
- 11 D. S. Jung, Y. N. Ko, Y. C. Kang and S. B. Park, *Adv. Powder Technol.*, 2014, **25**, 18–31.
- 12 J. Leng, Z. Wang, J. Wang, H.-H. Wu, G. Yan, X. Li, H. Guo, Y. Liu, Q. Zhang and Z. Guo, *Chem. Soc. Rev.*, 2019, **48**, 3015–3072.
- 13 K. Y. Jung, *RSC Adv.*, 2020, **10**, 16323–16329.
- 14 H. Min and K. Y. Jung, *Mater. Chem. Phys.*, 2021, **267**, 124612.
- 15 J. K. Kim, Y. Yoo and Y. C. Kang, *Chem. Eng. J.*, 2020, **382**, 122805.
- 16 H. Min and K. Y. Jung, *RSC Adv.*, 2017, **7**, 21314–21322.
- 17 S. Devesa, A. P. Rooney, M. P. Graca, D. Cooper and L. C. Costa, *Mater. Sci. Eng., B*, 2021, **263**, 114830.

